



**HAL**  
open science

# Seismic waves from atmospheric sources and Atmospheric/Ionospheric signatures of seismic waves

Philippe Lognonné

► **To cite this version:**

Philippe Lognonné. Seismic waves from atmospheric sources and Atmospheric/Ionospheric signatures of seismic waves. *Infrasound Monitoring for Atmospheric Studies*, Springer Netherlands, pp.281-304, 2010, 10.1007/978-1-4020-9508-5\_10 . hal-03917428

**HAL Id: hal-03917428**

**<https://u-paris.hal.science/hal-03917428>**

Submitted on 1 Jan 2023

**HAL** is a multi-disciplinary open access archive for the deposit and dissemination of scientific research documents, whether they are published or not. The documents may come from teaching and research institutions in France or abroad, or from public or private research centers.

L'archive ouverte pluridisciplinaire **HAL**, est destinée au dépôt et à la diffusion de documents scientifiques de niveau recherche, publiés ou non, émanant des établissements d'enseignement et de recherche français ou étrangers, des laboratoires publics ou privés.

# Seismic waves from atmospheric sources and Atmospheric/Ionospheric signatures of seismic waves.

**P. LOGNONNÉ**

*Institut de Physique du Globe de Paris, Equipe Géophysique Spatiale et Planétaire (UMR7154, IPGP, Université Paris Diderot CNRS), 4 Avenue de Neptune, 94100 Saint Maur des Fossés, France.*

[lognonne@ipgp.jussieu.fr](mailto:lognonne@ipgp.jussieu.fr)

## **Abstract**

The sounding of the ionosphere with GPS, Doppler sounder or Radar allows the detection of acoustic waves or gravity waves generated by quakes or tsunami at teleseismic distances, in addition to the acoustic waves generated by the seismic source near the epicenter. These waves are induced by the vertical displacement at the wave front of the Earth's surface. They propagate almost vertical, with an amplification with altitude associated to the exponential decay of the atmospheric density. For ground displacement of a few mm, acoustic waves amplitudes of a few tens to hundred meters are achieved at 250-300 km of altitude.

We review in this chapter the atmospheric coupling of these seismic waves, as well as the ionospheric/atmospheric coupling generating the ionospheric perturbations. We show that this coupling explains also the seismic signals generated by large atmospheric explosions. In both case, seismograms or ionograms can be modelled relatively accurately by normal modes summations techniques.

We finally discuss how the technological development in the last 10 years has lowered the detection threshold of ionospheric post-seismic signals and provides several perspectives that seem now to be possible by this new way of doing seismology without seismometers.

**Key Words:** seismology, ionosphere, lithosphere-atmosphere-ionosphere coupling, remote sensing, tsunami

## I. INTRODUCTION

Mikumo and Watada, in the previous chapter of this book, have presented in details the generation of acoustic-gravito waves by quakes and focused their discussion on the waves propagating mainly in the atmosphere, from the earthquake source to the atmospheric recording points. As noted in their section, if sound waves observations from local earthquakes are common, the observations of these waves by pressure sensors can be done worldwide only for magnitudes larger than 8

We focus in this chapter on the waves travelling mostly in the interior or liquid part of the Earth, but nevertheless with a smaller propagation path in the atmosphere. For atmospheric sources (e.g. atmospheric explosions), these waves propagate first in the atmosphere from up to downward, reach the ground and then propagate into the interior of the Earth. Alternatively, for solid earth sources (e.g. quakes), the waves propagate first in the solid earth, then reach the surface, and resume their propagation in the atmosphere, from the surface up to the ionospheric heights. In most cases, the propagation path in the atmosphere ranges from distances of 30km in the first case up to about 400-500 km in the second case, while the propagation in the interior of the Earth can be many thousands of km, the propagation being worldwide.

The other difference in our approach will be in the observational methods. While Mikumo and Watada are focusing on the observations in the atmosphere, we will concentrate our review on the observation of the waves at the end of their propagation path, and therefore on ionospheric observations, for waves generated by quakes, and on seismic observation, for waves generated by atmospheric sources.

Ionospheric observations, as we will see below, are especially interesting as they can be performed even for “small” magnitude quakes, as compared to the example of Mikumo and Watada in the range of  $M_s=8-9$ . The larger sensitivity of ionosphere as compared to the low atmosphere is attributed mainly to the exponential decay of the atmospheric density. The amplitudes of acoustic-gravity waves, when they propagate vertically, are indeed proportional to  $\rho(z) u^2$ , where  $\rho$  is the volumetric mass density and  $u$  the displacement of the atmospheric particles. When the frequency is lower than 10 mHz (or period larger than 100 sec), the atmospheric viscosity and heat conduction can be neglected up to altitudes of 120 km (Francis, 1973, Artru et al., 2001) and the amplitude is therefore increasing with altitude, inversely proportional to the square root of density. The resulting amplification can reach

factors of about  $10^4$  at 120 km of altitude and up to  $10^5$  at the altitudes of maximum ionization ( $\sim 300$  km), and made observations possible at short epicentral distances for magnitudes as low as 6, and worldwide for magnitudes of about 7.

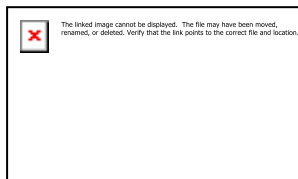
Many observations of these signals were reported after large quakes in Alaska or Japan in the 60th (Leonard and Bernes, 1965, Davis et Baker, 1965, Yuen et al., 1969, Weaver et al., 1970) with Doppler techniques sensitive to the vertical oscillations of the ionospheric layers. Much later, Calais et Minster (1995) reported ionospheric perturbations of the density of electrons by using another sounding method, based on data from Global Positioning System (GPS) receivers, and corresponding therefore to electron density perturbations. Since these works, the detection of the associated ionospheric perturbations has benefited from the recent developments in ionosphere remote sensing, in particular of techniques using GPS dense networks, Doppler HF sounder or even over-the-horizon radar. These tools provide unprecedented capabilities for monitoring the reaction of the ionosphere to seismic waves.

We present in this paper the state of the art in the modelling of these signals, with a review of the theory necessary to model the observations, and present and discuss the perspectives of this new seismological approach.

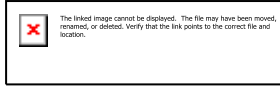
## **II. THEORETICAL MODELING OF THE SEISMIC WAVES IN THE NEUTRAL AND IONIZED ATMOSPHERE**

### **II. 1 SOLID EARTH-NEUTRAL ATMOSPHERE COUPLING**

The modelling of waves with a propagation path splitted in the Earth's interior and atmosphere has to take into account the two different media, and two approaches are therefore possible. In the first approach, one considers the surface of the Earth as a simple interface: when waves reach this interface, part of their energy is reflected, while the remaining part is transmitted, either in the atmosphere for up going waves or in the solid earth for down going waves. The transmission (t) and reflection (r) coefficients from the Earth's interior to the atmosphere can be easily estimated for waves propagating vertically:



while the energy transmission (T) and reflection (R) coefficients, which verify  $R+T=1$ , are



These simplified expressions, as well as the similar expression for a downward propagation, provide the order of magnitude of the energy transfer between the two systems, by using typical values for  $\rho_{\text{air}}, \rho_{\text{int}}, c_{\text{air}}$  and  $c_{\text{int}}$  (e.g. respectively  $1.2 \text{ kg/m}^3$ ,  $2600 \text{ kg/m}^3$ ,  $330 \text{ m/s}$  and  $5800 \text{ m/s}$  respectively). The energy transmitted by one transmission from the interior to the atmosphere or from the atmosphere to the interior is 4 times the acoustic impedance ratio between the air and interior, leading to about  $10^{-4}$  (Lognonné and Johnson, 2007). This will be typically the relative energy transferred by seismic body wave to the atmosphere or by an atmospheric source to the interior. Normal modes associated to seismic surface waves will transmit more energy, as they are stationary waves. The transmitted energy can however be estimated easily with this approach for the fundamental surface wave of angular order  $l$  easily with this approach. As they have a horizontal wavelength of  $\lambda$  and bounce on the surface one time per cycle, with an amplitude decreasing each time by  $e^{-Q}$  due to attenuation in the solid part, where  $Q$  is the quality factor of the mode, the total energy can be expressed as the sum of the term of a geometrical series  $\sum_{n=0}^{\infty} e^{-nQ}$ . During these successive bounces, the portion of energy transmitted to the atmosphere will therefore be  $\varepsilon \sum_{n=0}^{\infty} e^{-nQ}$ , where  $\varepsilon$  is the partition ratio between the energy in vertical displacement and the total energy, the latter being typically of the order of 0.5. For a  $Q$  value of 100, we find typical values of nearly  $10^{-3}$ , showing that almost one per mille of the energy of surface waves is dissipated in the Earth's atmosphere, as shown on Figure 1.

A much more detailed and rigorous theory is necessary for the modelling of the observed phenomena, especially due to the fact that most observations are done for long period seismic waves, with periods of several 10s of seconds or even a few of 100s of seconds, for which the high frequency approach of propagating waves and rays is not valid anymore: both the surface and the troposphere are indeed within one wavelength for acoustic waves of 100sec (i.e. about 30 km of wavelength). The first theory was developed by Watada (1995) and Lognonné et al. (1998). This approach takes into account the coupling between the solid Earth, the ocean and the atmosphere. In the latter paper, the boundary conditions of the elasto-dynamic operator at the solid Earth - atmosphere interface is integrated in the normal modes theory. A radiative boundary condition simulates the escape of acoustic and gravity atmospheric waves in the upper ionosphere, where no refraction of waves is observed.

Either variational methods (Lognonné et al., 1998) or iterative methods (Kobayashi, 2007) can be used, leading to the computation of normal modes with both eigenfrequency and eigenmodes with complex values. The dissipation related to viscosity in the atmosphere can be easily incorporated, as shown by Artru et al (2001). The integration of heat conductivity in a more exact way remains to be done in these simulations.

The results, for a typical atmospheric model (US standard atmospheric model, 1976) and the PREM model for the solid Earth (Dziewonski and Anderson, 1981) are shown in Figure 1. The finite wavelength of the long period acoustic waves generates resonance effects observed at the frequencies associated with the fundamental and overtones of the atmospheric wave-guide. At these frequencies (about 3.7 mHz and 4.44 mHz), a much larger fraction of the seismic waves is transferred in the atmosphere, and this preferential transmission is the major explanation not only for the bichromatic signals observed after volcanic eruptions, but also for the large ionospheric waves detected between 3.5 and 5 mHz. The amplitude of the normal modes, either in the atmosphere for the Rayleigh fundamental normal modes, or in the solid Earth for the acoustic normal modes, can be found in Lognonné et al., (1998), Lognonné and Clévéde (2002), Lognonné and Johnson (2007) and Kobayashi (2007). Figure 1 also provides a comparison of the coupling between the Earth and other telluric planets. This will be discussed briefly in section V.

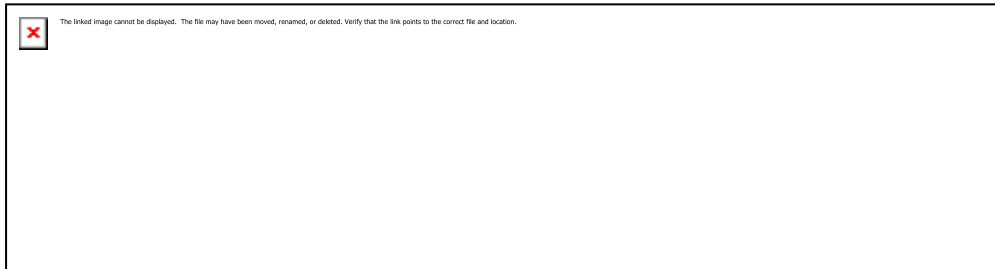
The properties of the atmospheric channel in this vertical propagation is however significantly dependent on the position and local time, as the structure of the atmosphere changes with position and local time (Figure 2). Both the energy transfer and the amplitudes of the normal modes are therefore affected. As the atmosphere/interior coupling is a local effect (i.e. associated with an horizontal propagation much smaller at long period than the wavelength of the seismic waves), a first modelling of this variability can be done by using the 1D theory described above on all point of the Earth surface, using on each of these points an empirical 2D atmospheric model, such as the NRLMSIS-00 model (Picone et al., 2000). The first feature observed is related to the crossing between the solid Earth fundamental Rayleigh modes (noted  ${}_0S$ ) and the atmospheric fundamental acoustic modes (noted  ${}_0P$ ). The latter is the main reason for the large energy transfer found around 3.7 mHz between the solid Earth and the atmosphere. Figure 3 shows that depending on the local time and location, this crossing can be either between the frequencies of  ${}_0S_{27}$ - ${}_0S_{28}$  or  ${}_0S_{28}$ - ${}_0S_{29}$ . This is generating a dependence of the energetic coupling with local time and location, as shown in Figure 4a: the amount of energy in the atmosphere can vary by a factor of two for the fundamental modes and the first overtones at the resonances frequency and the amplitudes are found to be the

largest during the night, when the acoustic impedance of the atmosphere is the highest (Figure 4b).

As a first step, spherically symmetric normal modes can be used to compute, with a summation technique, not only seismograms from atmospheric sources, but also atmospheric signals from quakes. We however have to keep in mind the effect of the atmospheric variability, which will require the computation of normal modes for a 3D time dependant atmosphere for more precise studies.


## II.2 NEUTRAL ATMOSPHERE -IONOSPHERIC COUPLING

When atmospheric waves reach the ionosphere, they interact with the ionospheric plasma. This interaction is done mainly through collision processes, which transfer the velocity of the neutral atmosphere, noted as  $\delta w$  to the ions or electron. The electrons/ions are then interacting through electromagnetic forces in order to maintain the ionosphere neutrality and Electric field and Magnetic field are therefore perturbed. Both ions and electrons in addition interact with the magnetic and electric fields, and to the first order, the velocity of the charged particles is then significant only along the direction of the magnetic field (Dautermann et al., 2008, Ostrovsky, 2008, Kherani et al., 2009). More in details, the Fourier transform of the velocity of a given ionized species can be expressed as (Kherani et al., 2009)



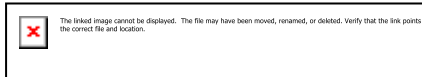
where we use the Fourier transformed components of the velocity of a given species  $\delta u$  and  $b_r, b_\theta$  and  $b_\phi$  are the direction cosines of the magnetic field along the  $r, \theta$  and  $\phi$  directions.



is the ratio between the gyropulsation of the ionized species and its collision frequency,  is the ratio between the pulsation of the wave and the collision frequency

and the final expression are given to the first order of  $1/\kappa$ .  $q$  and  $m$  are the charge and mass of the species, while  $B$  is the local amplitude of the magnetic field and  $i$  is such that  $i^2=-1$ . The typical values of the collision frequencies are given on Figure 5, while the gyrofrequency ( $2\pi$  time smaller than the pulsation) is about 1.4 MHz for electrons and a 50 000 nT magnetic

field amplitude, typical of the Earth magnetic field over California or Japan. The gyrofrequency is 30 000 times smaller for the O<sup>+</sup> ion and therefore about 45 Hz. This shows that for both ions and electrons,  $\kappa$  is much larger than unity, and for the surface waves,  $\eta$  is smaller than unity, which justify these expressions valid to the first order in  $1/\kappa$ . The ionospheric perturbation in velocity is therefore mainly parallel to the magnetic field and has a smaller component perpendicular to the magnetic field. The electron density variations are expressed by the conservation equation




in the linearized case and when no perturbation in the production rate is assumed. Here  is the background and steady state electron current, such as the Equatorial electro-jet. These effects are generating both latitudinal and azimuthal effects on the ionospheric signals.

Figure 6 shows the latitudinal effect, for typical amplitudes recorded in the ionosphere, for surface arbitrary vertical amplitude of one mm in displacement, at the frequency of 5 mHz. We note the amplification with altitude of the neutral wave, as well as its latitude dependence related to change of the scale height between the equator and poles. Due to the magnetic field, the vertical charged velocity is cancelling at the magnetic equator while the maximum in the electron density perturbation is found at the equator, with a secondary maximum at mid-latitudes. Figure 6 also illustrates that the ionospheric perturbation cannot be recorded everywhere with the same efficiency and tools and that both Doppler sounder (sensitive to the velocities) and GPS sounders (sensitive to the electron density) are necessary to perform observations over a wide range of latitudes.

This azimuth dependence of electron density perturbation is illustrated in Figures 7a and 7b, for an acoustic expanding wave, generated over Japan, where the magnetic inclination is about 50°. During its perturbation, the acoustic ray is bended due to the increase of the sound speed. When propagating southward, it reaches therefore a point where it is parallel to the magnetic field, while a perpendicular configuration is in contrary found for northward propagation path. This azimuth sensitivity, leading to an apparent directivity effect on the observations of ionospheric-seismic signals from quakes (Heki and Ping, 2005) or of ionospheric-acoustic signals from volcanic eruptions (Heki, 2006) must be taken into account for any amplitudes modelling and interpretation.



### III OBSERVATION AND INVERSIONS

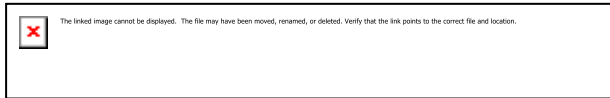
Our review will focus on the observations performed relatively far from the source, when the contributions from the waves propagating in the atmosphere and excited at the source by the ground displacement can be separated from the seismic tele-seismic waves. We will therefore not cover the ionospheric observations of the direct acoustic waves, the latter being the high altitude counter part of the waves described in detail by Mikuma and Watada. These waves have however been reported and in some cases modeled by many studies (e.g. Afraimovich et al., 2001, Heki and Ping, 2005, Kiryushkin et al., 2007, Heki et al., 2006, Astafyeva and Afraimovich, 2006, Shinagawa et al., 2007) and where probably the waves detected originally by Calais and Minster (1995). We will also not review the possible atmospheric origin of the “hum” of Earth’s free oscillation, as the oceanic waves are probably the major source of its excitation (Webb, 2007). See however Tanimoto and Artru (2007) for a recent review on the possible atmospheric contribution to this “hum”.

#### III.1 ATMOSPHERIC COUPLING AT THE SOURCE

The first illustration of the seismic/acoustic wave coupling can be found in signals detected in an atmosphere-Earth’s interior path, in which the Rayleigh waves (and theoretically body waves too) are excited at the source by powerful atmospheric sources. They then can propagate in the solid Earth over long distances. The typical sources for such signals are the volcanic explosions, like El Chichon in 1982, Pinatubo in 1991 and more recently Montserrat in 2003.

The first clear observation was made after the Pinatubo eruption: by stacking 12 IDA stations records of 12 hours long, Zürn & Widmer (1996) have shown indeed that the recorded signals have a selective excitation of Rayleigh surface waves around frequencies of 3.7 mHz and 4.44 mHz for the two main peaks. Many papers were published on the explanation of these unusual signals. Some have proposed a feedback regime between the atmosphere and the volcano (Widmer & Zürn, 1992, Zürn & Widmer, 1996). Others proposed the excitation of two atmospheric waves, the low frequency one being a gravity wave, and the other being acoustic (Kanamori & Mori, 1992, Kanamori et al., 1994). It is now recognized that this bichromatic excitation is simply related to the fact that the Rayleigh waves with frequencies around 3.7 mHz and 4.44 mHz have more energy in the atmosphere and are therefore more excited than the others.

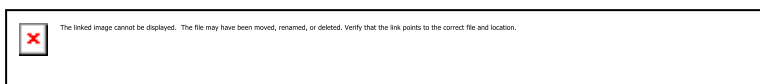
Such view can be consolidated by a waveform source inversion of the Pinatubo data, shown in Figure 8, where 18 stations of the Global Network (Geoscope and Iris) on the VLP channels corresponding to the full day of June, 15, 1991 are arranged. In such inversion, we have to compute the seismograms, by using the Rayleigh normal modes with their atmospheric extension, as shown in Figure 5. A standard normal mode summation technique (e.g. Lognonné, 1991) can be used. For an explosive force, the expression of the seismograms is given by Lognonné et al. (1994):

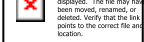


where  $\mathbf{r}_s$  and  $\mathbf{r}_e$  are the receiver, explosion coordinates respectively, index  $k$  denotes a given mode with quantum numbers  $l, m, n, \sigma_k$  and  $\mathbf{u}_k$  are the normal frequency and normal mode respectively associated to index  $k$ . The source term  $M_k(\mathbf{r}_e, t)$  is given by the source integrated over the whole source volume and is expressed by  $M_k(t) = V_s \Delta p(t) \text{div}(\mathbf{u}_k)$  when the source is represented as an isotropic pressure glut  $\Delta p(t)$  in the source volume  $V_s$ . Note that in the source term, the divergence of the normal mode eigenfunction is taken at the source location  $\mathbf{r}_e$ . The pressure glut is defined, following Lognonné et al. (1994) as the difference between the true pressure and the Hooke pressure plus the Reynolds stresses.

Such an expression allows therefore to test the source altitude. Figure 9 shows the result of a least square inversion of the data with synthetics filtered in the frequency bandpass window from 1 mHz to 8 mHz, assuming that the seismic source is localized at a given altitude  $z$  (or depth  $-z$ ), being isotropic in all direction and radiating during 10 hours starting after June, 14, 1991.

The inversion is performed by least square fitting of the vertical ground displacement after instrumental correction and by adding a correlation time to the moment tensor history, in order to stabilize the inversion. We therefore minimize



with an exponential correlation function , in order to stabilize this inverse problem. Inversions for all altitudes from a few kilometers depth to about 60 km of altitude are then performed and compared. The best variance reduction (about 60 %) is found near the surface and at an altitude between 24 and 28 km (Figure 10a-b). In these two cases, the physical meaning of the seismic source is therefore different, with simple models of mass

injection for the surface source and more complex models of shock waves for the altitude source. See for example *Lognonné et al., 1994* for a detailed analysis of the seismic radiation of shock waves generated by explosion. In order to assess the validity of a low altitude source with respect to a high altitude one, the amplitudes of the two different sources can be compared. The seismic moment minimum value is  $M_0 = \tau_b (\gamma - 1) E$  (Lognonné et al., 1994), where  $\gamma$  is the adiabatic index of the atmosphere,  $\tau_b$  the duration of the blast and  $E$  the energy released. The maximum value is  $M_0 = 2 \tau_b E$ , when all the energy  $E$  is released in kinetic energy, which might be the case for an eruption where most of the ejecta have a vertical velocity. As shown in Figure 10b reasonable amplitudes are found only for a source at 24-28 km of altitude, with most of the energy released at the time of the individual explosions. These releases of seismic moment are found near the reported date of the individual eruptions. These eruptions are equivalent to yields of about 4000 MT.sec, corresponding to explosions releasing about 20 MT during blast times of about 200-500 sec, which corresponds to the order of magnitude of the Pinatubo eruption, whose energy is about 200 MT in several explosions. These results show that the seismic source of the Pinatubo eruption can be relatively well explained by a series of eruptions rather than the complex mechanisms proposed by the previous studies.

In a similar approach, Dautermann et al (2008a, 2009) have recently studied the 2003 Montserrat eruption associated with the explosive lava dome collapse of the Soufriere Hills volcano. Both signal in the ionosphere, associated to the acoustic wave and detected on the TEC GPS data, and signals in the ground, associated to the seismic waves and detected on strain sensors, have been recorded. As for the Pinatubo, best results in the waveform fitting are achieved for a source in the atmosphere. Note however that in these case, both the acoustic and seismic waves must be taken into account in the modelling, as the observations are too close for achieving a separation of the wavetrains, as it was the case for the remote seismic signals of the Pinatubo eruption.

### **III.2 IONOSPHERIC-ATMOSPHERIC COUPLING OF SEISMIC WAVES**

Let us now consider the same coupling processes, but in the opposite propagating direction, i.e. from the Earth's interior toward the Earth's atmosphere. The classical example will here be a quake, generating seismic waves converted partially to atmospheric waves when the seismic wave front reaches the Earth's surface. In this process, only horizontal S

waves, i.e. SH or Love waves, will not generate acoustic waves. All others will be converted and acoustic waves will therefore be launched into the atmosphere for incident SV and P body waves and also for the spheroidal surface waves, especially the fundamental Rayleigh ones.

The amplitudes of the acoustic waves are generally quite small at the Earth's surface (Their amplitude, for vertically incident waves, is twice the amplitude of the vertically incident seismic waves from the Earth's interior). The typical amplitude of the associated pressure waves in the atmosphere can be estimated, for a vertically incident body wave, to



for the typical values of the density and sound speed of the atmosphere at the ground level. For travelling surface waves and for nearly-horizontally travelling body waves from shallow earthquakes, the pressure wave is twice smaller (e.g. Watada et al., 2006). This shows that even for 20 sec surface waves of 1 mm amplitude, corresponding to the typical surface waves from large ( $M_s > 8$ ) quakes at teleseismic distance, the pressure fluctuation is a fraction of Pa. The same is observed for body waves: one second body waves of  $1 \text{ cm/s}^2$ , corresponding to the acceleration of a local and shallow  $M=3.5$  quake or to a Mercalli scale of II, generates ground amplitudes of  $250 \text{ }\mu\text{m}$  and a corresponding pressure fluctuation smaller than 0.25 Pa. These amplitudes are one order of magnitude smaller than those of the records studied by Mikumo and Watada in the previous section, which correspond to large quakes (e.g.  $M_s > 8$ , such as the 2003 Tokachi-Oki earthquake studied by Watada et al., 2006). This shows the difficulties for observing signals for most of the quakes at the ground level and the importance of the amplification in the acoustic waves amplitudes observed when the latter propagate upward towards the ionospheric height, where they are amplified due to the atmospheric density decay.

During more than 4 decades, the detected signals described above were more or less considered as some “funny” or “exotic” observation in seismology, unable to provide new valuable informations, either on the source or on the internal structure of the Earth. However, we are now facing a rapid improvement, with the development of new technologies in ionospheric sounding, or with the progressive development of dense GPS networks. This puts a new light on these researches and starts to point out possible seismological interests and applications.

Following the pioneering works done with analogue Doppler sounder (Davis and Baker, 1965; Leonard and Barnes, 1965; Row, 1966, 1967; Yuen et al, 1969) observations

have been continuously done with improved performances (Namazov et al., 1975, Najita and Yuen, 1979, Tanaka et al., 1984, Blanc, 1985, Egorov et al, 1990, Parrot et al., 1993). The new generations of sounders, such as the Doppler sounder operated by CEA/DASE in France can detect most of the earthquakes with  $M_s$  greater than 6.5 (Artru et al., 2004). They provide data very similar to seismograms in the sense that they measure directly the vertical motion of an ionospheric layer: both surface waves and body waves are detected in the ionosphere, including SV waves (see Fig 11). Many other Doppler sounder are in operation and have collected a large amount of data, especially after the large Sumatra quake with observations in Taiwan (Liu et al., 2006), China (Hao et al., 2006) in addition to those in France. A close analysis of these data however shows that the propagation of the signal at high altitudes is not well explained by acoustic propagation only and that the observed propagation velocities are much lower than the acoustic values (Artru et al., 2005). In Figure 11, this might be observed when we compare the 1 min delay between the waveforms at 186 km and 168km, with the theoretical delay of about 30 sec. The full understanding of these data will therefore need further works.

These Doppler instruments still remain limited to a small number of point measurements and cannot resolve the 3D structure of the perturbation. Recent studies have therefore used Over-The-Horizon radars, which might provide maps of the ionospheric vertical displacements (Occhipinti, 2006), including the detection of the R2 phase of the Rayleigh waves generated by the Sumatra, March 28  $M_s=8.7$  earthquake (Occhipinti et al., 2008). Preliminary results show that the signal to noise ratio of these instruments is probably comparable to those obtained by Doppler sounders and that these instruments could therefore be a way to provide dense measurements of the seismic wavefront, with sampling as low as 1 measurement per 25 km<sup>2</sup> over Earth's surface of several 10<sup>6</sup> km<sup>2</sup>. Their use for scientific application remains however challenging.

Another approach is necessary. It can be based on electron density perturbation measurements performed by the GPS networks (see Manucci 1998 for details on the ionospheric sounding with GPS and Lognonné et al., 2006 for a review on its seismic applications). The first seismic observations were performed by Calais and Minster (1995) after the 1994 Northridge earthquake ( $M_s=6.7$ ), who detected perturbations in the ionospheric total electron. Afraimovich *et al.* (2001) detected the acoustic shock waves associated with two earthquakes that occurred in Turkey in 1999. Ducic et al (2003) have then used data from the dense California GPS networks and detected the ionospheric Rayleigh waves. As Najita and Yuen (1979), they were able to use the ionospheric perturbations for the computation of

the group velocity of the long period oceanic Rayleigh waves. The 3D structure of the Denali ionospheric signal was then characterized by Garcia et al. (2005) and with such approach, the comparison of signals from identical altitude can be performed. Figure 12 illustrates these 3D views of the ionospheric signal and confirms experimentally the maximum electron density altitude, as compared to Figure 6.

The dense and denser GPS networks available around the world, especially in Japan, California and USA and Europe, allow now numerous observations. Figure 12 shows one such example, following the shallow (depth = 27 km), Tokachi-Oki earthquake of September, 25, 2003 ( $M_s=8.3$ , latitude of  $41.775^\circ\text{N}$  and longitude of  $143.904^\circ\text{E}$ ). We clearly see on this profile the transition at an epicentral distance of about 200 km between the acoustic waves, propagating mainly in the atmosphere with an acoustic velocity smaller than 1000m/s, and the acoustic signature of the Rayleigh waves, with an apparent velocity corresponding to the seismic Rayleigh surface waves (3500 m/s).

Much more studies will probably be made in the near future on the seismological analysis of these data: in addition to the group velocity measurement already done by Najita and Yuen (1979) and Ducic et al. (2003), we can in particular envisage new seismic source constrain, following the first studies done by Heki and Ping (2005), Kiryushkin et al. (2007) for the 2003 Tokachi-Oki quake and and and Heki et al. (2006) or Shinagawa et al (2007) for the large 2004 Sumatra quake.

#### **IV. IONOSPHERIC-ATMOSPHERIC COUPLING OF TSUNAMI WAVES**

As for surface waves, early observations (Donn and Mc Guinness, 1960) and theoretical works (Peltier and Hines, 1976) predicted that atmospheric gravity waves are generated in the wake of a tsunami through resonant coupling between atmospheric and water gravity waves. About 30 minutes are needed for the gravity wave to develop its first maximum perturbation in the ionosphere (versus ~10 minutes for seismic-acoustic waves). But after this delay the ionospheric perturbation follows the tsunami front and, as for the seismic waves, the atmospheric oscillations are amplified with altitude. It should also be noted that, due to their much shorter wavelength and period, the surface noise of ocean swell does not produce significant upward propagating waves into the atmosphere: the atmosphere acts as a filter, enhancing the long wavelength tsunami perturbation over other sources. Figure 14 shows the results of simulation, where the tsunami first generates an atmospheric gravity wave that is

then generating, through collisions between neutral atmosphere and ions, perturbations in the electronic density.

The first ionospheric observation had however to wait almost 30 years. It was made after the Peru, June, 2001 tsunami (Artru et al., 2005). The tsunami arrival was observed on Japanese tide gauges between 20 and 22 hours after the earthquake, with wave amplitudes between 10 and 40 cm (open ocean amplitude were estimated to be of 1-2 cm) and dominant periods of 20 to 30 minutes. Shortly after, a large ionospheric perturbation was detected through a specific processing of data from the continuous GPS network in Japan (GEONET). The arrival time, orientation, wavelength, velocity of the wave packet observed are consistent with what is expected for a tsunami-induced perturbation.

The gigantic and dramatic Sumatra tsunami of December, 2004 confirmed the possibilities of observing tsunami-induced ionospheric signals, which were actually detected on the Total Electronic Content (TEC) measurement on-board the TOPEX/Poseidon and JASON satellites. The modelling of the ionospheric signal shows that both the waveform and the amplitude observed by Jason and Topex can be reproduced (Occhipinti et al., 2006). Improved modeling have been done by taking into account the magnetic field (Occhipinti et al., 2008), the dissipation/diffusion processes (Mai and Kiang, 2009) and Coriolis and height dependent winds (Hickey et al., 2008). Other observations were performed worldwide, either on GPS data in the India Ocean (Lognonné et al., 2006, DasGupta et al., 2006, Liu et al., 2006, Otsuka et al., 2006) or even at the Aricebo facility (Lee et al., 2008). All these signals can be associated with the ionospheric perturbation attributed to the propagating tsunami. These results confirm the interest of a real-time monitoring of the ionosphere, which could be carried out either with active microwave radar or by optical systems for airglow detection. They open new prospect for future tsunami warning techniques.

## **V. EXPORTING REMOTE SENSING SEISMOLOGY ON VENUS?**

Although on the Earth the technique described above would never provide the same quality of seismic data as a seismic network, they can be a unique way to obtain seismic data on planets too hostile for the deployment of long-lived seismic stations. Venus is the best example (Garcia et al., 2006, Lognonné and Johnson, 2007). In addition, the coupling strength is proportional to the acoustic impedance of the atmosphere, equal to  $\rho c$  where  $\rho$  is the density and  $c$  the acoustic speed. As the atmospheric density at the surface of Venus is

about  $60 \text{ kg/m}^3$  and the acoustic velocity is slightly higher (410 m/s) than on the Earth, this leads to an acoustic impedance about 60 times greater than on the Earth, where the atmospheric density is  $1.2 \text{ kg/m}^3$ .

Moreover, at an altitude of 50 km, where the Venus pressure is comparable to Earth ground pressure, the decrease by almost 2 order of magnitude of the density leads already to an amplification of 10 of the acoustic waves. Consequently, Venus quakes will generate atmospheric infrasonic waves with amplitudes much larger than on the Earth surface (Figure 16). This profitable effect gives a unique opportunity for a future detection of Venus quakes by a satellite sounding the Venus ionosphere.

## **VI. CONCLUSION**

A significant coupling between the acoustic and seismic waves is observed. This coupling is well understood theoretically. It generates remote seismic waves excited by large atmospheric sources and atmospheric and ionospheric signals coupled to the seismic wavefront. This coupling explains most of the signals recorded by the large volcanic eruption, which occurred in the last three decades. It also explains the ionospheric signals, made available by the recent advance in the monitoring of small-scale perturbations of the ionosphere: Rayleigh waves, tsunami-induced gravity waves and even seismic body waves generate signals which can be observed by ionospheric sounding based on GPS network, Doppler sounder, OTH radars and Spaceborne dual-frequency altimeter sounding. These new data open exciting prospects in seismology such as the remote sensing of the seismic Rayleigh wave fronts especially over the ocean, where the deployment of dense seismic networks is the most challenging. These techniques might also provide in a future a high-resolution picture of the wave front of body waves. These prospects are also very exciting for tsunamis because the latter are extremely difficult to observe in the open ocean. The tsunami generated atmospheric gravity waves have a clear impact on the ionosphere and can be detected by remote sensing systems. Other applications of this technique are also found in planetology, especially with interesting prospects in the remote sensing of quakes on Venus.

## **VII. ACKNOWLEDGEMENT**

I thank J.Artru, V.Ducic, F.Crespon, R.Garcia, A.Kherani, G.Occhipinti and L.Rolland for their contributions to the development of the ionospheric seismology project in IPGP



L.Rolland, F.Crespon, R.Garcia, G.Occhipinti and A.Kherani are acknowledged for providing some figure of this review. I thank T.Farges for making available Doppler data from CEA and two anonymous reviewer for constructive comments. This work was funded by CNES, ESA and ANR. This is IPGP contribution xx.

## VIII REFERENCES

Afraimovich, E.L., Perevalova, N.P., Plotnikov, A.V., Uralov, A.M., 2001. The shock-acoustic waves generated by the earthquakes. *Annales Geophysicae* 19, 395–409.

Artru J., P. Lognonné et E. Blanc, 2001. Normal modes modeling of post-seismic ionospheric oscillations. *Geophysical Res. Lett.*, 28, 697-700.

Artru, J. T. Farges, P. Lognonné, 2004. Acoustic waves generated from seismic surface waves: propagation properties determined from Doppler sounding observation and normal-modes modeling, *Geophys. Jour. Int.*, 158, 1067-1077.

Artru, J., V. Ducic, H.Kanamori, P. Lognonné and M. Murakami, 2005. Ionospheric detection of gravity waves induced by tsunamis, *Geophys. J. Int*, 160, 840-848, doi : 10.1111/j.1365-246X.2005.02552.x2005.

Astafyeva EI, Afraimovich EL, 2006. Long-distance traveling ionospheric disturbances caused by the great Sumatra-Andaman earthquake on 26 December 2004, *Earth Planets and Space.*, 58, 1025-1031.

Bilitza, D. (2001). International reference ionosphere 2000, *Radio Science*, 36, 261-275.

Blanc, E., 1985. Observations in the upper atmosphere of infrasonic waves from natural or artificial sources: A summary, *Annales Geophysicae*, 3 (6), 673-688.

Calais, E., & Minster, J. B., 1995. GPS detection of ionospheric perturbations following the January 17, 1994, Northridge earthquake, *Geophys. Res. Lett.*, 22, 1045-1048.

DasGupta, A., A. Das, D. Hui, K.K. Bandyopadhyay and M.R. Sivaraman (2006), Ionospheric perturbation Observed by the GPS following the December 26th, 2004 Sumatra-Andaman earthquake, *Earth Planet. Space*, 35, 929-959.

Dautermann, T., E. Calais, and G. Mattioli (2008), GPS Detection, Modeling and Energy Estimation of the Ionospheric Wave caused by the 2003 Explosion of the Soufriere Hills Volcano, Montserrat, *J. Geophys. Res.*, 114, B02202, doi:10.1029/2008JB005722.

Dautermann, T. E. Calais, P. Lognonné, G.S. Mattioli, 2009. Lithosphere-Atmosphere-Ionosphere Coupling after the 2003 Explosive eruption of the Soufriere Hills Volcano, Montserrat, *Geophys. J. Int.*, 179, 1537-1546, doi:10.1111/j.1365-246X.2009.04390.x

Davies, K., and D.M. Baker, 1965. Ionospheric effects observed around the time of the Alaskan earthquake of March 28, 1964. *Journal of Geophysical Research*, 70, 1251-1253.

Davies, J.B and C.B.Archambeau, 1998. Modeling of atmospheric and ionospheric disturbances from shallow seismic sources, *Phys. Earth Planet. Inter.*, 105, 183-199.

Donn, W.L. and McGuinness, W.T., 1960. Air-Coupled Long Waves in the Ocean, *J. of Atmospheric Sciences*, 17, 515-521.

Ducic, V. J. Artru and P. Lognonné, 2003. Ionospheric remote sensing of the Denali Earthquake Rayleigh surface waves. *Geophys. Res. Lett.*, 30(18), 1951, doi:10.1029/2003GL017812.

Dziewonski A. and D.L. Anderson, 1981. Preliminary reference Earth model, *Phys. Earth Planet. Inter.*, 25, 297-356.

Forget, F; F. Hourdin, R. Fournier, C. Hourdin, O. Talagrand, M Collins, S. Lewis, Stephen R.; P.L. Read, J-P. Huot, 1999. Improved general circulation models of the Martian atmosphere from the surface to above 80 km, *J. Geophys. Res.*, **104**, 24155-24176

Garcia, R., F. Crespon, V.Ducic, P. Lognonné, 2005. 3D ionospheric tomography of the Denali seismo-acoustic waves over California, *Geophys. J. Int*, **163**, 1049-1064, 2005, doi : [10.1111/j.1365-246X.2005.02775.x](https://doi.org/10.1111/j.1365-246X.2005.02775.x).

Garcia, R., P.Lognonné and X.Bonnin, 2005. Detecting atmospheric perturbations produced by Venus quakes, *Geophys. Res. Lett.*, **32**, L16205, doi : [10.1029/2005GL023558](https://doi.org/10.1029/2005GL023558).

Garcia R.F. and F. Crespon, 2008, Radio tomography of the ionosphere: Analysis of an under-determined, ill-posed inverse problem, and regional application., *Radio Science*, 43, RS2014, doi:10.1029/2007RS003714

Hao, YQ; Xiao, Z; Zhang, DH, 2006. Responses of the ionosphere to the Great Sumatra earthquake and volcanic eruption of Pinatubo, *Chinese Physics Letters*, 23, 1955-1957.

Heki, K. 2006. Explosion energy of the 2004 eruption of the Asama Volcano, central Japan, inferred from ionospheric disturbances, *Geophys Res Lett.*, **33**, doi: 10.1029/2006GL026249.

Heki, K., and J. Ping, 2005. Directivity and apparent velocity of the coseismic ionospheric disturbances observed with a dense GPS array, *Earth Planet. Sci. Lett.*, **236**, 845 – 855.

Heki, K., Y. Otsuka, N. Choosakul, N. Hemmakorn, T. Komolmis, and T. Maruyama 2006. Detection of ruptures of Andaman fault segments in the 2004 great Sumatra earthquake with coseismic ionospheric disturbances, *J. Geophys. Res.*, 111, B09313, doi:10.1029/2005JB004202.

Hickey, M. P.; Schubert, G.; Walterscheid, R. L., Simulations of Tsunami Effects in the F-Region Ionosphere, American Geophysical Union, Fall Meeting 2008, abstract #SA21B-1547

Huba J.D., Joyce and J.A. Fedder (2000), Sami2 is another model of the ionosphere (SAMI2): A new low-latitude ionosphere model, *J. Geophys. Res.* **105**, 23 035.

Hunten, D. M., L. Colin, and T. M. Donahue, 1983. Venus, 1143 pp., Univ of Ariz. Press, Tucson.

Kanamori, H., and Mori, J., 1992. Harmonic excitation of mantle Rayleigh waves by the 1991 eruption of mount Pinatubo, Philippines, *Geophys. Res. Lett.*, 19, 721-724.

Kanamori, H., J. Mori and D.G. Harkrider, 1994. Excitation of atmospheric oscillations by volcanic eruptions. *J. Geophys. Res.*, **22**, 21947-21961.

Kherani, E.A. P. Lognonné, N. Kamath, F. Crespon and R. Garcia, 2009. Fluctuations in ionosphere during seismic activity, *Geophys J. Int.*, 176, 1-13, doi: 10.1111/j.1365-246X.2008.03818.x

Kiryushkin, VV, Afraimovich, EL, 2007. Determining the parameters of ionospheric perturbation caused by earthquakes using the quasi-optimum algorithm of spatiotemporal processing of TEC measurements, *Earth Planets And Space*, 59, 267-278.

Kobayashi, Naoki, A new method to calculate normal modes, 2007, *Geophys. J. Int.*, 168, 315-331.

Lee, M. C., R. Pradipta, W. J. Burke, A. Labno, L. M. Burton, J. A. Cohen, S. E. Dorfman, A. J. Coster, M. P. Sulzer, and S. P. Kuo (2008), Did Tsunami-Launched Gravity Waves Trigger Ionospheric Turbulence over Arecibo?, *J. Geophys. Res.*, 113, A01302, doi:10.1029/2007JA012615.

Leonard, R.S. and R.A. Barnes, Jr., 1965. Observation of ionospheric disturbances following the Alaska earthquake, *J. Geophys. Res.*, **70**, 1250.

Liu, J. Y., Y. B. Tsai, S. W. Chen, C. P. Lee, Y. C. Chen, H. Y. Yen, W. Y. Chang and C. Liu (2006a), Giant ionospheric disturbances excited by the M9.3 Sumatra earthquake of 26 December 2004, *Geophys. Res. Lett.*, **33**, L02103.

Liu, J., Y. Tsai, K. Ma, Y. Chen, H. Tsai, C. Lin, M. Kamogawa, and C. Lee (2006b), Ionospheric GPS total electron content (TEC) disturbances triggered by the 26 December 2004 Indian Ocean tsunami, *J. Geophys. Res.*, **111**, A05303. 52

Lognonné P., 1991. Normal modes and Seismograms of an anelastic rotative Earth., *J. Geophys. Res.*, **96**, 20309-20319.

Lognonné, P., B. Mosser and F.A. Dahlen, 1994. Excitation of the Jovian seismic waves by the Shoemaker-Levy 9 cometary impact, *Icarus*, **110**, 186-195.

Lognonné, P., C. Clévéde and H. Kanamori, 1998. Normal mode summation of seismograms and barograms in a spherical Earth with realistic atmosphere. *Geophys. J. Int.*, **135**, 388-406.

Lognonné P. and E. Clévéde, 2002. Chapter 10: Normal modes of the Earth and Planets, In: H. Kanamori, P. Jennings and W. Lee (Eds.), Handbook on Earthquake and Engineering Seismology, IASPEI Centennial Publications, International Geophysics series, 81A, Academic Press.

Lognonné P., Juliette Artru, Raphael Garcia, François Crespon, Vesna Ducic, Eric Jeansou, Giovanni Occhipinti, Jérôme Helbert, Guilhem Moreaux, Pierre-Emmanuel Godet, Ground based GPS tomography of ionospheric post-seismic signal., *Planet. Space. Science*, **54**, 528-540, doi : [10.1016/j.pss.2005.10.021](https://doi.org/10.1016/j.pss.2005.10.021), 2006

Lognonné P. and C. Johnson, Planetary Seismology, Treatise in Geophysics, G. Schubert, editor, Elsevier, section 10.04, 2007

Mai, C.L. and Kiang, J.F., Modeling of Ionospheric Perturbation by 2004 Sumatra Tsunami, *Radio Science*, submitted, 2009.

Mannucci, A. J., 1998. A global mapping technique for GPS-derived ionospheric electron content measurements, *Radio Science*, **33**, 565-582.

Najita, K. & Yuen, P., 1979. Long-period Rayleigh wave group velocity dispersion curve from HF Doppler sounding of the ionosphere, *J. Geophys. Res.*, **84**, 1253-1260.

Namazov, S. A.; Novikov, V. D.; Khmel'nitskii, I. A., 1975. Doppler frequency shift in ionospheric propagation of decametric radio waves, *Radiofizika*, **18**, 473-500.

Occhipinti, G., Observations multi-paramètres et modélisation de la signature ionosphérique du grand séisme de Sumatra, Ph.D. Thesis, Institut de Physique du Globe de Paris, December 2006.

Occhipinti, G., P. Lognonné, E. Kherani, H. Hébert, 2006. 3D Waveform modeling of ionospheric signature induced by the 2004 Sumatra tsunami, *Geophys. Res. Lett.*, 33, L20104, doi : [10.1029/2006GL026865](https://doi.org/10.1029/2006GL026865).

Occhipinti, G., E.A. Kherani, P. Lognonné, 2008. Geomagnetic dependence of ionospheric disturbances induced by tsunamigenic internal gravity waves, *Geophys. J. Int.*, 753-755, 173, doi : 10.1111/j.1365-246X.2008.03760.x.

Occhipinti, G., Farge, T.; Dorey, P.; Lognonné, P., Nostradamus: the Radar that wanted be a Seismometer, American Geophysical Union, Fall Meeting 2008, abstract #S43D-1916

Ostrovsky, L.A, 2008. Ionospheric effects of ground motion: The roles of magnetic field and nonlinearity, *J. of Atmos. and Solar-Terrest. Physics*, **70**, 1273-1280

Otsuka Y, Kotake N, Tsugawa T, Shiokawa K, Ogawa T, Effendy, Saito S, Kawamura M, Maruyama T, Hemmakorn N, Komolmis T, 2006. GPS detection of total electron content variations over Indonesia and Thailand following the 26 December 2004 earthquake, *Earth Planets And Space*, 58, 159-165 .

Parrot M, Achache J, Berthelier J.J., Blanc E, Deschamps A, Lefeuvre F, Menvielle M, Plantet J.L., Tarits P, Villain J.P, 1993. High-frequency seismo-electromagnetic effect. *Phys. Earth Planet Int.* 77, 65–83.

Peltier, W. R. & C. O. Hines, 1976. On the possible detection of tsunamis by a monitoring of the ionosphere. *J. Geophys. Res.*, 81(12), 1995–2000.

Picone, J.M., A.E. Hedin, D.P. Drob, and A.C. Aikin, 2002. NRLMSISE-00 empirical model of the atmosphere: Statistical comparisons and scientific issues. *J. Geophys. Res.*, 107, (A12), 1468, doi:10.1029/2002JA009430.

Row, R.V., 1966. Evidence of Long-Period Acoustic-Gravity Waves Launched into the F Region by the Alaskan Earthquake of March 28, 1964, *J. Geophys. Res.*, 71, 343–345.

Row, R. V., 1967. Acoustic-Gravity Waves in the Upper Atmosphere Due to a Nuclear Detonation and an Earthquake, *J. Geophys. Res.*, 72(5), 1599–1610.

Shinagawa, H., Iyemori, T., Saito, S. and Maruyama, T., 2007. A numerical simulation of ionospheric and atmospheric variations associated with the Sumatra earthquake on December 26, 2004, *Earth, Planets and Space*, 59, 1015-1026.

Tanaka, T., T. Ichinose, T. Okuzawa, T. Shibata, Y. Sato, C. Nagasawa, T. Ogawa, 1984. HF-Doppler observation of acoustic waves excited by the Urakawa-Oki earthquake on 21 March 1982. *J. Atmo. Terr. Phys.*, 46, 3, 233-245.

Tanimoto, T. and J. Artru (2007), Interaction of Solid Earth, Atmosphere, and

Ionosphere, *Treatise on Geophysics, Vol. 4*, 421-444.

U.S. Standard atmosphere, 1976. Committee on the extension to the Standard atmosphere, U.S. Government printing office, Washington D.C.

Watada, S. (1995), Part 1: Near source acoustic coupling between the atmosphere and the solid earth during volcanic eruptions, Ph.D. thesis, California Institute of Technology

Watada, S; Kunugi, T; Hirata, K, Sugioka H, Nishida K, Sekiguchi S, Oikawa J, Tsuji Y, Kanamori H, 2006. Atmospheric pressure change associated with the 2003 Tokachi-Oki earthquake, *Geophys. Res. Lett.*, 33, L24306.

Webb, S.C, 2007. The Earth's 'hum' is driven by ocean waves over the continental shelves, *Nature* 445, 754-756

Weaver, P. F., Yuen, P. C., Prolss, G. W., and Furumoto, A. S., 1970. Acoustic coupling in the ionosphere from seismic waves of the earthquake at Kurile Islands on August 11, 1969. *Nature*, 226, 1239-1241.

Widmer, R., and Zürn, W., 1992. Bichromatic excitation of long-period Rayleigh and air waves by the mount Pinatubo and El Chichon volcanic eruptions, *Geophys. Res. Lett.*, 19, 765-768.

Woodhouse, J.H. & Dziewonski, A.M., 1984. Mapping the upper mantle: three dimensional modelling of earth structure by inversion of seismic waveform, *J. Geophys. Res.*, 89, 5953-5986.

Yuen, P. C., Weaver, P. F., Suzuki, R. K., and Furumoto, A. S., 1969. Continuous traveling coupling between seismic waves and the ionosphere evident in May 1968 Japan earthquake data. *J. Geophys. Res.*, 74, 2256-2264.

Zürn, W. and R. Widmer, 1996. World wide observation of bichromatic long-period Rayleigh-waves excited during the June 15, 1991 Eruption of Mt. Pinatubo. In : C. Newhall, R. Punongbayan (Ed.), *Fire and Mud, Eruptions of Mount Pinatubo, Philippines*, Philippin Institute of Volcanology and Seismology, Quezo City and University of Washington Press, 615-624.



**Figure 1:** Fraction of the energy of surface waves in the Venus, Earth and Mars atmospheres for Rayleigh surface waves. Only the first peaks are due to atmospheric resonances. Note that the amplitudes on Mars and Earth are comparable at low frequency (2-3 mHz), due to differences in the atmospheric resonance frequency. US standard atmospheric model (1976) is used for the Earth, whereas the models of Forget *et al.* (1999) and Hunten *et al.* (1983) are used for Mars and Venus respectively (Reprinted from Lognonné and Johnson, 2007).

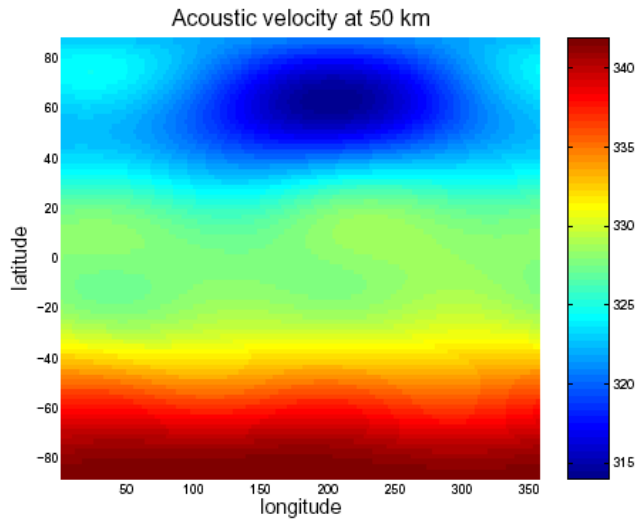


**Figure 2 :** Sound speed in the atmosphere for model NRLMSISE-00 on January 1<sup>st</sup>, a 0h00 TU, as a function of altitude and longitude, at an altitude of 50 km. Variations are about 10% peak-to-peak

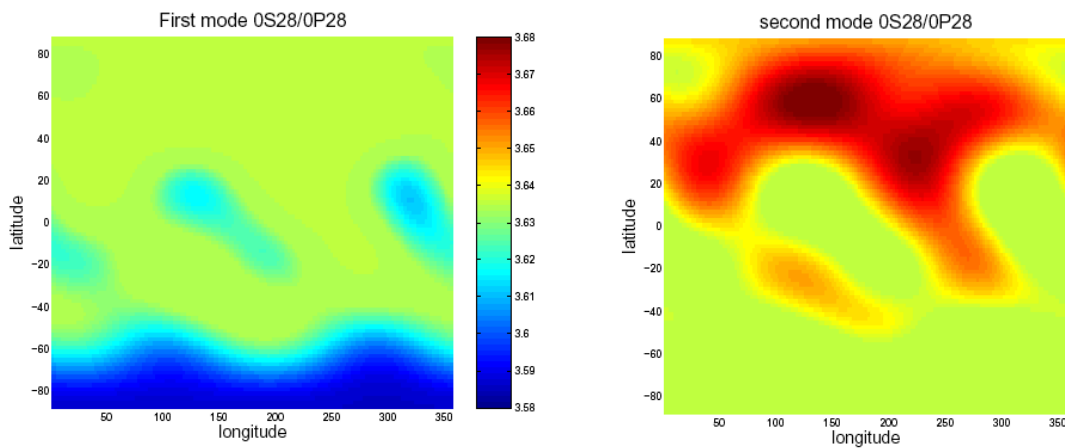


**Figure 3 :** Left: Location of the Earth where the fundamental atmospheric acoustic mode  ${}_0P_{28}$  has a frequency below the frequency of the fundamental Rayleigh seismic mode  ${}_0S_{28}$ . The values of the frequency, with colour scale in mHz, is given in color, the one of  ${}_0S_{28}$  being the middle green value of the colour scale. Right: The figure shows the location of the Earth where the fundamental atmospheric acoustic mode  ${}_0P_{28}$  has a frequency higher than the frequency of the fundamental Rayleigh seismic mode  ${}_0S_{28}$ . The frequency of  ${}_0S_{27}$ ,  ${}_0S_{28}$  and  ${}_0S_{29}$  are 3.544 mHz, 3.635 mHz and 3.726 mHz respectively, showing that the acoustic mode is either between  ${}_0S_{27}$  and  ${}_0S_{28}$  or  ${}_0S_{28}$  and  ${}_0S_{29}$ , depending on the location.



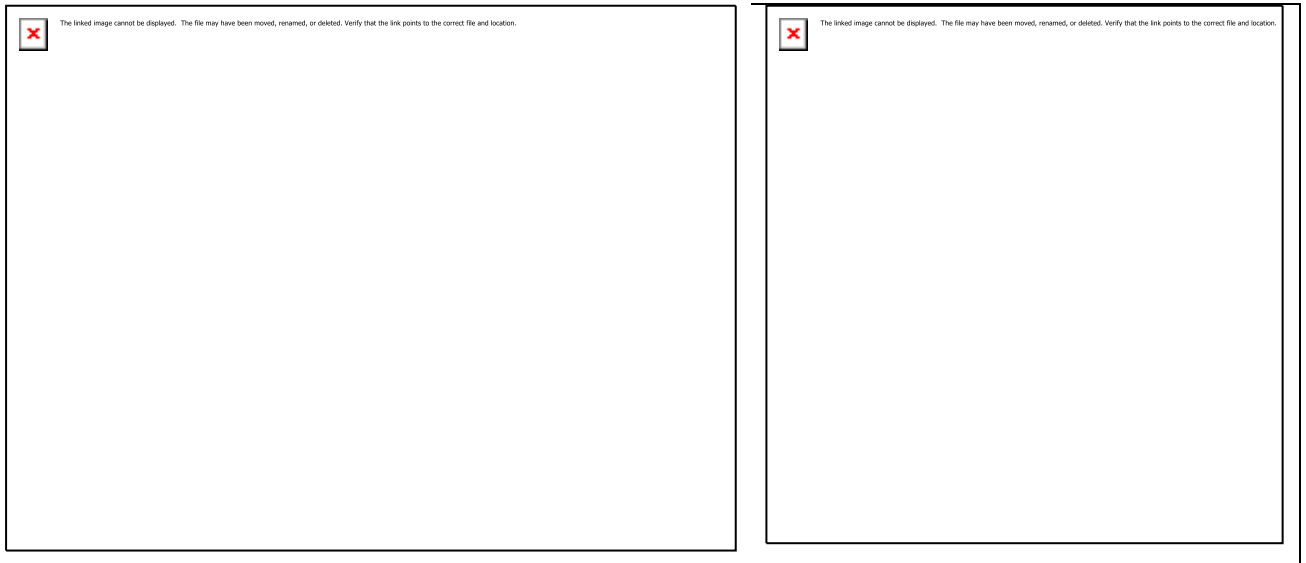


**Figure 4a-b:** (a) Left: Plot of the fraction of energy in the atmosphere for the fundamental Rayleigh waves of angular order up to 50 and for the first harmonics, for different local time of the MSISE-00 atmospheric model. The interior model remains PREM for all cases. The resonances, while occurring for different angular orders, are found at the same frequencies. Right: plot of the amplitude of the vertical component of the fundamental Rayleigh waves near the resonance (angular order 29). The amplitudes, multiplied by the square root of density, are multiplied by 100 in the atmosphere. A minimum of coupling is found near 12h local time.

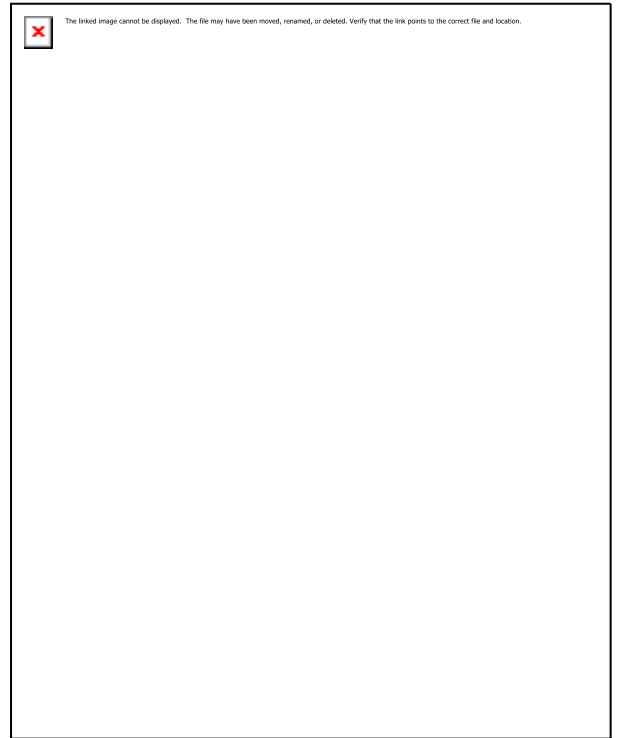


**Figure 5:** (left) Typical electron density as obtained from IRI (Bilitza et al., 1996) for a morning condition (5h local time). Right Figure shows the typical collision frequencies for ion-neutral and electron-neutral, as obtained from model SAMI2 (Huba et al., 2001)

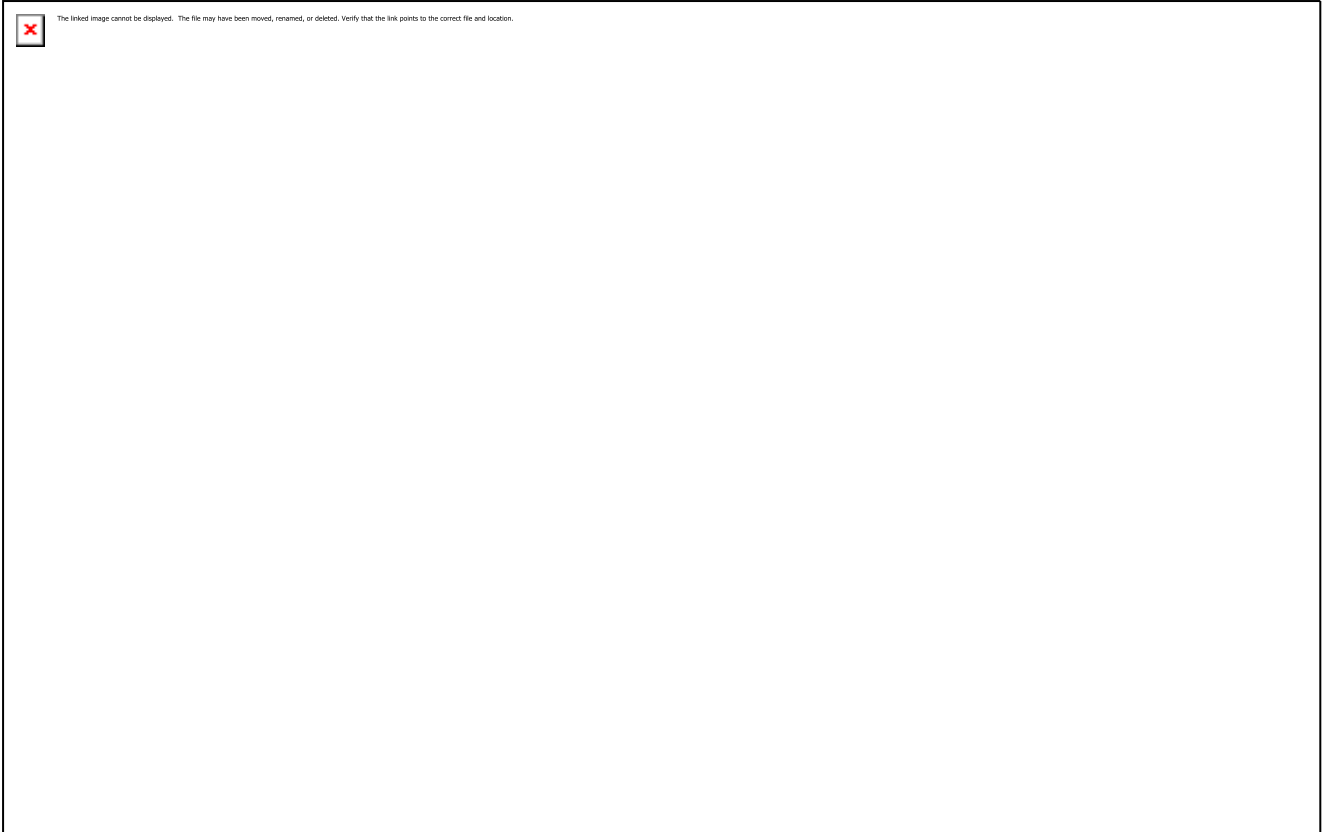


**Figure 6:** Left and middle figures are the electron density and electron vertical velocity responses to the neutral velocity of the right figure. This neutral velocity field takes into account the amplification of acoustic waves with altitude and its dissipation at high altitude. The period of the acoustic wave is set to 200 sec and IRI and SAMI2 models (see Figure 5) are used for the computation of the perturbations. From Kherani et al., 2009.

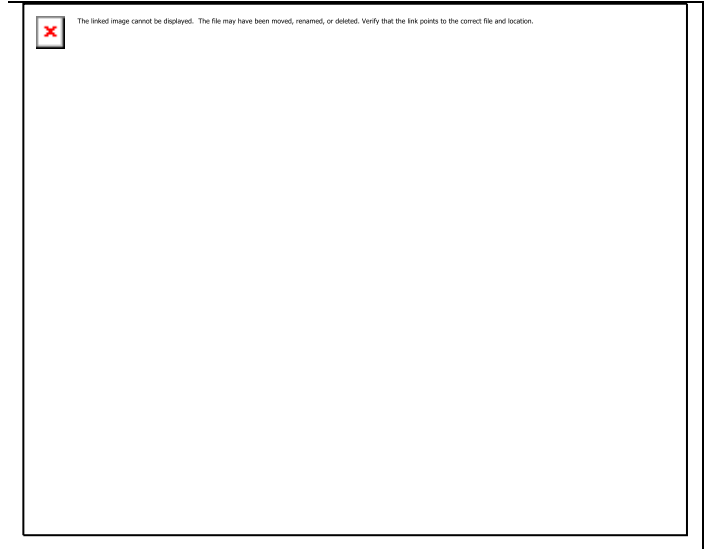


**Figure 7a-b:** 3D simulation of an acoustic wave generated by a point source at the surface, over Hokkaido, Japan. X and Y direction are along west east and south north respectively. The left figure shows the isotropic perturbations in electron density when no magnetic field is taken into account. They reach a maximum at the maximum ionization altitude. The right figure shows the effect of the magnetic field, which focus the perturbation in the south, where the acoustic rays reach a configuration parallel to the magnetic field.

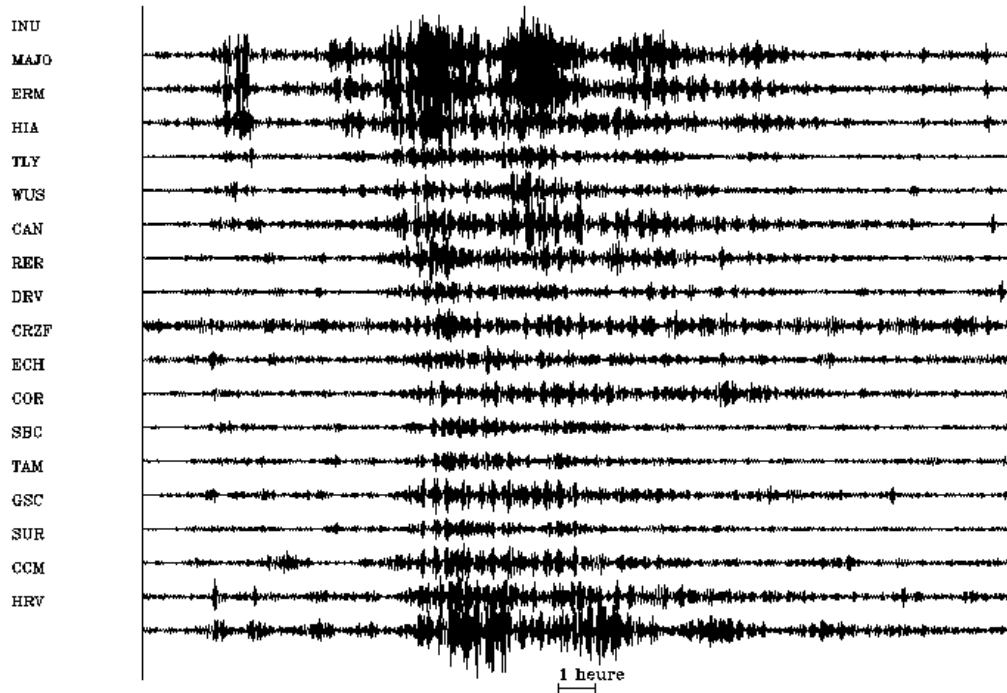


**Figure 8** : Bandpass filtered vertical data recorded after the Pinatubo eruption by several station of the global network. Stations have increasing epicentral distance from top to bottom. The Two small quakes recorded on the data and originating from other sources as the Pinatubo region (A  $M_s=6.1$  quake from Causasus and a  $M_s=6.3$  quakes from South Sandwich Islands, occurring respectively at 0059TU and 0113TU) are subtracted from the data after CMT inversion of both quakes achieved by a waveform fitting of coupled synthetics computed for the M84A aspherical model (Woodhouse and Dziewonski, 1984).

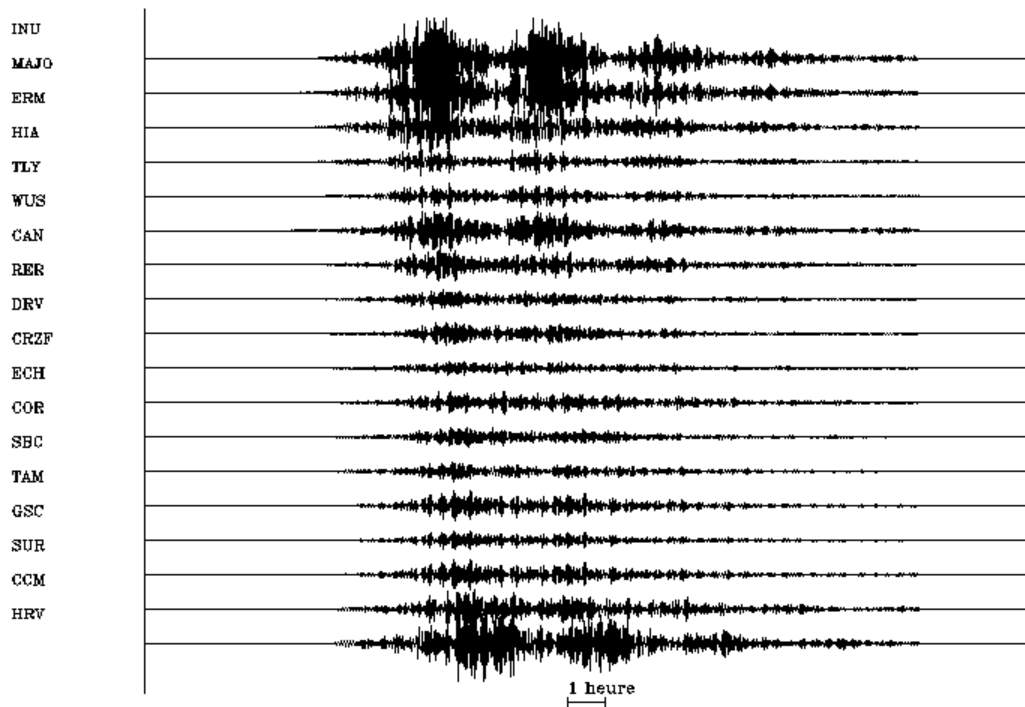


**Figure 9:** Synthetics found in the inversion, explaining 60% of the variance of the data. The fundamental and the ten first overtones were taken in the normal modes summation and all the normal modes of these branch in the studied frequency window where taken. Note that the main characteristics of the waveforms are retrieved, as well as amplitudes.



**Figure 10a** : variance reduction for a series of inversion, for different values of altitude and weighting factor. The best sources are found either at the ground level in the atmosphere or at an altitude between 20-28 km corresponding to the altitude reached by the eruptions.

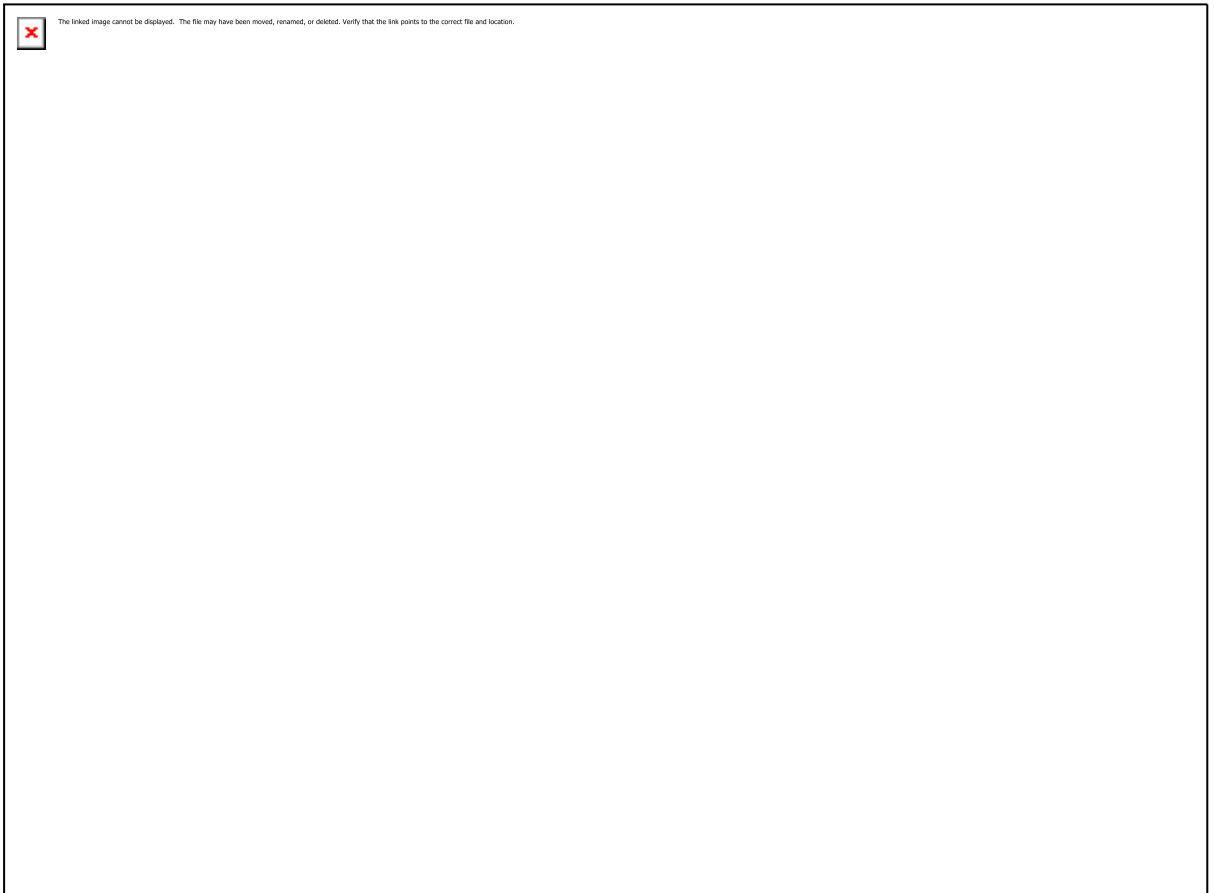


**Figure 10b:** Source history for a surface pressure glut versus time. Amplitude is in 20 MT of equivalent TNT times one second. The source is at 28 km of altitude, and when compared to the source solution for a shallow atmospheric source, the amplitude of the source is reduced by a factor 100 as well as the complexity of the source. The obtained source function is closer from a series of explosion, each of them of about 20-40 MT and with burst times of the order of 200-500 sec. Vertical lines are associated to the reported eruption of the volcano and several fits with the burst found in the source function.





**Figure 11:** Seismic surface waves after the  $M_w = 7.6$  Chi-Chi earthquake (Taiwan, September 20, 1999) as measured on a ground seismometer (bottom panel) at the Geoscope station SSB (Saint-Sauveur, France) and on the CEA ionospheric Doppler sounding network (Francourville, France), corresponding to the vertical motion of ionospheric layers at altitudes 168 and 186 km. These two stations are located at  $89.06$  and  $89.17^\circ$  of epicentral distance. All traces show the vertical velocity perturbation in the 1-50 mHz frequency band. An amplification of  $4 \cdot 10^4$  is observed between the ground and the ionosphere. The  $\sim 8$  minutes delay between the ground and the ionosphere at 168 km of altitude corresponds to the propagation time of the acoustic wave. About 28 sec are necessary from 168 km to 186 km. Due to this delay, body waves are expected to arrive in the ionosphere at about 18h20, 18h26 for S and SS waves respectively, while surface waves arrive at about 18h39'30''. SV waves, due to SV-P conversion are therefore possibly detected. Comparison with synthetics obtained with normal modes can be found in Artru et al. (2005). Adapted from Tanimoto and Artru (2006)



The linked image cannot be displayed. The file may have been moved, renamed, or deleted. Verify that the link points to the correct file and location.

**Figure 12:** Acoustic and Rayleigh waves detected by the Japanese Geonet GPS network after the Tokachi-Oki earthquake of September, 25, 2003. Data are filtered in the bandpass 2.4-4 mHz, where the atmospheric coupling is the largest. The two grey lines are hodochrons for waves propagating at 3.5 km/s and 1 km/s from the source. Amplitudes are in TEC units. Up to about 300 km of epicentral distance, acoustic waves, propagating mainly in the atmosphere, are detected, while Rayleigh waves appear clearly at distances larger than 300 km.



**Figure 13:** Vertical cut of the 3D Rayleigh waves impact in the ionosphere for the Tokachi-Oki event. The Total Electronic Content amplitudes observed are typically 0.1 TECU peak-to-peak but 3D local variations reach a few  $10^9$  e/m<sup>3</sup>. No wavefront is observed with a north or northwest propagation direction, due to a poor coverage of the GPS satellite in these directions. The 3D reconstruction is done following methods of Garcia et al. (2005) and Garcia and Crespon (2008).

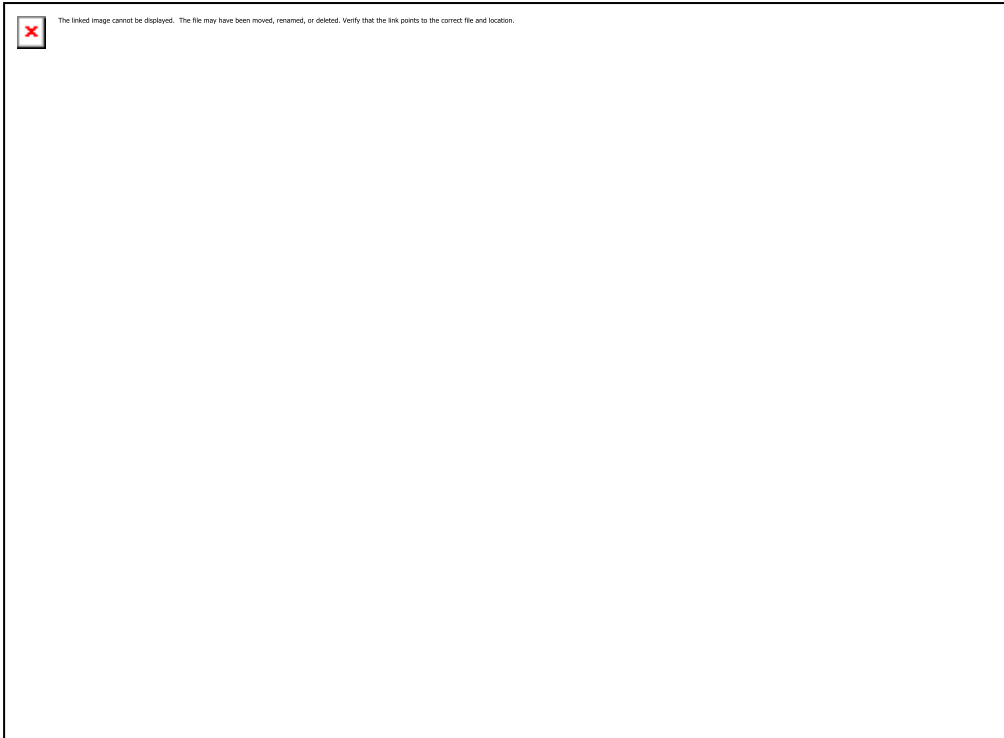


**Figure 14:** Coupling between the neutral atmosphere gravity wave induced by a tsunami and the ionosphere. The tsunami amplitude has a 0.5 meter amplitude and about 13min period, corresponding to the amplitude of the 2004 Sumatra tsunami. From top to below are the normalised neutral wind, and the absolute and relative electron density. This shows that perturbations up to 10% are generated by such tsunamis. From Occipinti et al. [2008]

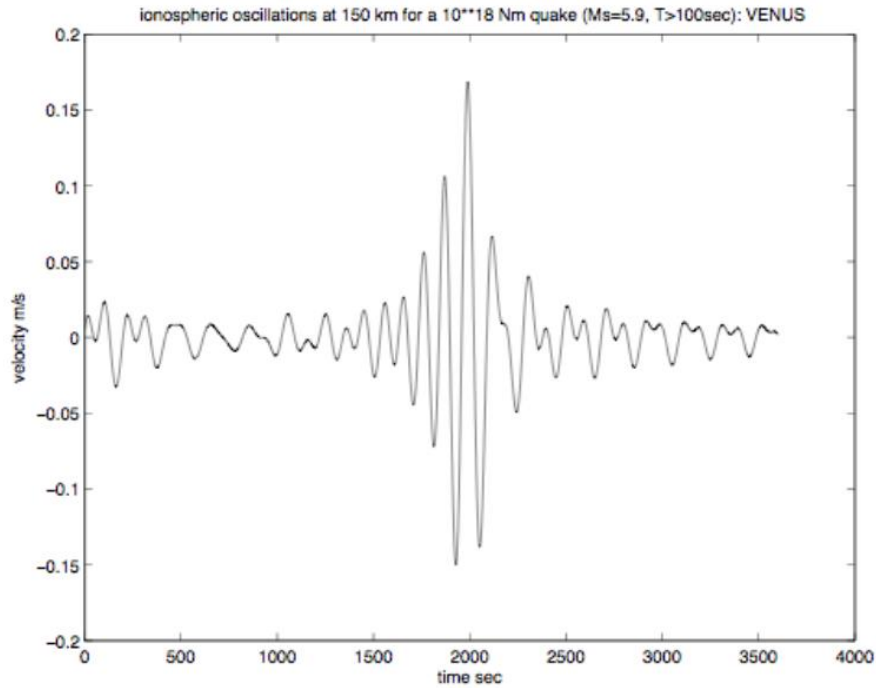


**Figure 16:** Long period vertical atmospheric oscillations, for a  $10^{18}$  Nm quake ( $M_w=5.9$ ) and for period larger than 100 sec on Venus. Due to the difference in the acoustic coupling at the ground, ionospheric signals at 150 km of altitude are about 100 stronger on Venus for the same magnitude and altitude than on Earth.